ERDC TR-23-4

US Army Corps
of Engineers®
Engineer Research and
Development Center

Exploration of Two Polymer Nanocomposite Structure-Property Relationships Facilitated by Molecular Dynamics Simulation and Multiscale Modeling

William A. Pisani, Dane N. Wedgeworth, Michael R. Roth,
John K. Newman, and Manoj K. Shukla

March 2023

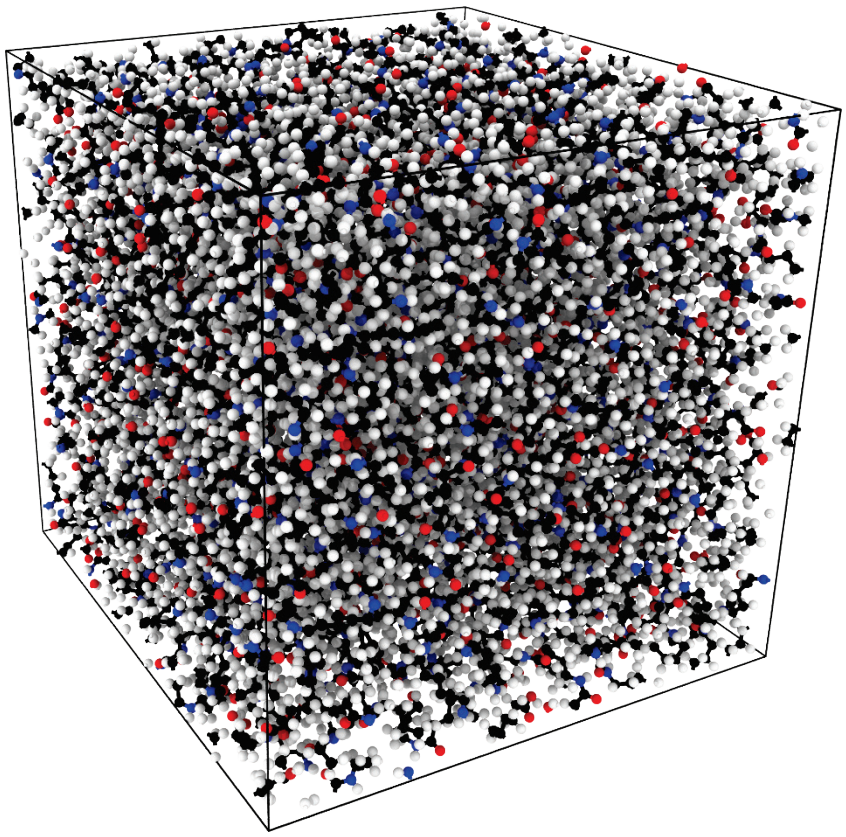

Engineer Research and
Development Center

The US Army Engineer Research and Development Center (ERDC) solves the nation's toughest engineering and environmental challenges. ERDC develops innovative solutions in civil and military engineering, geospatial sciences, water resources, and environmental sciences for the Army, the Department of Defense, civilian agencies, and our nation's public good. Find out more at www.erdc.usace.army.mil.

To search for other technical reports published by ERDC, visit the ERDC online library at https://erdclibrary.on.worldcat.org/discovery.

ERDC TR-23-4
March 2023

Exploration of Two Polymer Nanocomposite Structure-Property Relationships Facilitated by Molecular Dynamics Simulation and Multiscale Modeling

William A. Pisani, Michael R. Roth, and Manoj K. Shukla

Environmental Laboratory
US Army Engineer Research and Development Center
3909 Halls Ferry Road
Vicksburg, MS 39180-6199

Dane N. Wedgeworth and John K. Newman

Geotechnical and Structures Laboratory
US Army Engineer Research and Development Center
3909 Halls Ferry Road
Vicksburg, MS 39180-6199

William A. Pisani

Oak Ridge Institute for Science and Education
1299 Bethel Valley Road
Oak Ridge, TN 37830-8007

Final report

Prepared for Geotechnical and Structures Laboratory
US Army Engineer Research and Development Center
Research Group, CEERD-GMR
3909 Halls Ferry Road
Vicksburg, MS 39180-6199

Under Program Element Number PE 0602144A; Project Number 497006; Task Number 5L9C47

Abstract

Polyamide 6 (PA6) is a semi-crystalline thermoplastic used in many engineering applications due to good strength, stiffness, mechanical damping, wear/abrasion resistance, and excellent performance-to-cost ratio. In this report, two structure-property relationships were explored. First, carbon nanotubes (CNT) and graphene (G) were used as reinforcement molecules in simulated and experimentally prepared PA6 matrices to improve the overall mechanical properties. Molecular dynamics (MD) simulations with INTERFACE and reactive INTERFACE force fields (IFF and IFF-R) were used to predict bulk and Young's moduli of amorphous PA6-CNT/G nanocomposites as a function of CNT/G loading. The predicted values of Young's modulus agree moderately well with the experimental values. Second, the effect of crystallinity and crystal form (α/γ) on mechanical properties of semi-crystalline PA6 was investigated via a multiscale simulation approach. The National Aeronautics and Space Administration, Glenn Research Center's micromechanics software was used to facilitate the multiscale modeling. The inputs to the multiscale model were the elastic moduli of amorphous PA6 as predicted via MD and calculated stiffness matrices from the literature of the PA6 α and γ crystal forms. The predicted Young's and shear moduli compared well with experiment.

Contents

List of Figures

Preface

This study was conducted for the Geotechnical and Structures Laboratory, US Army Engineer Research and Development Center (ERDC), Research Group, under Program Element Number PE 0602144A; Project Number 497006; Task Number 5L9C47. The technical monitor was Dr. Elizabeth Ferguson.

The work was performed by the Environmental Chemistry Branch of the Environmental Processes and Engineering Division, ERDC, Environmental Laboratory. At the time of publication of this report, Ms. Amber L. Russell was branch chief; Mr. Warren P. Lorentz was division chief; and Dr. Elizabeth Ferguson was the technical director for Installations and Operational Environments. The deputy director of Environmental Laboratory was Dr. Brandon Lafferty, and the director was Dr. Edmond J. Russo.

The authors acknowledge the High-Performance Computing resources at the US Army Engineer Research and Development Center, Army Research Laboratory, and Michigan Technological University for computational time to perform this research.

The commander of ERDC was COL Christian Patterson, and the director was Dr. David W. Pittman.

This page intentionally left blank.

1 Introduction

1.1 Background

Polyamide 6 (PA6) is a semi-crystalline thermoplastic used in many engineering applications due to high strength, good chemical resistance, and excellent wear/abrasion resistance. A thorough understanding of the molecular structure-mechanical properties relationship is necessary to design improved PA6 composite materials. CNT/G possess excellent mechanical properties: both possess a Young's modulus of approximately 1 TPa [1, 2] and have specific strengths greater than steel. CNT/G have outstanding potential as reinforcement to polymer matrices and have been increasingly used to improve the strength/stiffness-to-weight ratios of polymer composites (Qian et al. 2000; King et al. 2013). Several studies have investigated the effect of CNT/G reinforcement of PA6 on some mechanical properties (strength, elastic, and shear moduli, etc.) (Liu et al. 2004; Tahreen and Masud 2013; Park et al. 2020; Liu et al. 2012; Xu et al. 2006; Yu et al. 2020; Zhou et al. 2015; Fu et al. 2015; Mayoral et al. 2015; Méndez et al. 2017; Shao et al. 2006; Wang et al. 2020), but little is known about the effect of CNT/G reinforcement on the bulk modulus of PA6 nanocomposites because the bulk modulus of solid materials is extraordinarily difficult to measure experimentally. While quite difficult to measure experimentally, bulk modulus is easily predicted computationally using molecular dynamics (MD) simulation. The bulk modulus of a solid material is an important property because a material's response to pressure waves is dependent upon the bulk modulus.

MD simulation is an accurate, efficient tool for predicting mechanical properties of bulk polymers and their composites (Hadden et al. 2013; Odegaard et al. 2014; Hadden et al. 2015; Chinkanjanarot et al. 2018; Radue et al. 2018a; Radue et al. 2018b; Pisani et al. 2019; Al Mahmud et

[1] For a full list of the spelled-out forms of the units of measure used in this document, please refer to *US Government Publishing Office Style Manual*, 31st ed. (Washington, DC: US Government Publishing Office 2016), 248-52, https://www.govinfo.gov/content/pkg/GPO-STYLEMANUAL-2016/pdf/GPO-STYLEMANUAL-2016.pdf.

[2] For a full list of the unit conversions used in this document, please refer to *US Government Publishing Office Style Manual*, 31st ed. (Washington, DC: US Government Publishing Office 2016), 345-7, https://www.govinfo.gov/content/pkg/GPO-STYLEMANUAL-2016/pdf/GPO-STYLEMANUAL-2016.pdf.

al. 2019; Patil et al. 2020; Pisani et al. 2021a). In this report, the INTERFACE (IFF) and reactive INTERFACE force fields (IFF-R) were used in the MD simulations. IFF excels at predicting interfacial properties of polymer and CNT/G reinforcements accurately and efficiently (Dharmawardhana et al. 2017; Heinz et al. 2013). IFF-R excels at predicting mechanical properties of polymers and their composites (Heinz 2021; Winetrout et al. 2021; Odegard et al. 2021; Pisani et al. 2021b).

The mechanical properties of semi-crystalline PA6 are dependent on two forms of crystallinity (α/γ) (Fornes et al. 2003; Sun et al. 2007; Murthy 1991; Phang et al. 2006; Bureau et al. 2002). These two crystal forms are created due to PA6's tendency to maximize the hydrogen bonding between chains (Fornes and Paul 2003). The difference between the two forms is in how the PA6 chains are hydrogen bonded (Fornes and Paul 2003; Zhu et al. 2014). For the α form, the chains are fully extended; for the γ form, the chains are twisted. The density of α form is 1.23 g cm^{-3}, and the density of γ form is 1.16 g cm^{-3} (Fornes and Paul 2003); the density of amorphous PA6 is 1.084 g cm^{-3}. Unfortunately, only a few studies report on both mechanical property and crystallinity values of PA6 (Mayoral et al. 2014; da Paz et al. 2016; Faghihi et al. 2015), and fewer still report on the specific type of crystal form present within the samples (Bureau et al. 2002). Most studies in the open literature do not report quantitative data on mechanical properties and the associated crystallinity values (Shan et al 2007; Shan et al. 2009; Gu et al. 2013). These studies have limited usefulness to computational modeling studies, which rely on quantitative experimental data to validate the modeling. The authors believe that comprehensive studies on the effect of crystallinity and crystal forms on the mechanical properties of PA6 do not exist.

The microstructure of semi-crystalline polymers is hierarchical and multiscale; from smallest to largest unit, this multiscale hierarchy exists as folded chains of polymer, granular substructures, lamellae stacks, spherulites, and the root network (Strobl 2006; Su et al. 2016; Jian et al. 2009; Wang et al. 2016; Ivanov et al. 1999; Hudson et al. 1992; Mills et al. 2020, 49–66). However, due to the computational complexity, fully atomistic MD simulations are limited to the nanoscale and thus cannot be used to model the hierarchical, multiscale microstructure of semi-crystalline polymers directly. The National Aeronautics and Space Administration (NASA) Glenn Research Center developed a micromechanics tool called Micromechanics Analysis Code based on the

Generalized Method of Cells (MAC/GMC) (Bednarcyk and Arnold 2002, 2). MAC/GMC contains a module called MultiScale Generalized Method of Cells (MSGMC) that can couple an arbitrary number of representative unit cells (of arbitrary complexity) across many length scales to determine thermo-mechanical properties of the overall multiscale structure. The MAC/GMC and MSGMC computational techniques have been validated across multiple studies (Hadden et al. 2015; Pisani at al. 2019; Cross et al. 2018; Gustafson et al. 2019; Tomasi et al. 2019; Ricks et al. 2109; Höwer et al. 2019).

1.2 Objective

In this work, the authors sought to understand how (1) the addition of carbon nanotubes and graphene sheets to PA6 changed the mechanical properties of the polymer matrix and (2) the crystallinity and crystal form of PA6 affects the mechanical properties of semi-crystalline PA6.

1.3 Approach

There are two structure-property relationships explored in this study. The first structure-property relationship is the effect of CNT/G loading on the mechanical properties of amorphous PA6. This report presents the approach for establishing well-equilibrated amorphous PA6-G and amorphous PA6-CNT nanocomposites with IFF and IFF-R. The predicted Young's and bulk moduli of amorphous PA6-CNT/G nanocomposites are presented. Experimental data were used to validate the predicted Young's moduli. For the second structure-property relationship, a previously validated multiscale modeling approach, originally developed for semi-crystalline polyetheretherketone (PEEK) (Pisani 2019), was used, which combined MD-predicted amorphous mechanical properties, crystalline mechanical property values from literature, and MSGMC to predict mechanical properties of semi-crystalline PA6 as a function of crystallinity and crystal form. The multiscale model predictions showed that the mechanical properties of semi-crystalline PA6 with α and γ crystal forms are similar from amorphous to 40% crystalline and diverge after this limit, with the γ PA6 predictions having higher Young's and shear moduli and lower Poisson's ratio. The Young's and shear moduli predictions agree well with experiment, validating the modeling.

2 Methods

2.1 Molecular dynamics modeling

2.1.1 General simulation information

The open-source MD code LAMMPS (19 March 2020 version) was used (Plimpton 1995); the time-step was set to 1.0 femtoseconds (fs) for all simulations. All visualizations of the atomic structure were performed with the OVITO software (Stukowski 2010). The non-reactive class 2 IFF was used for densifying, polymerizing, and equilibrating the neat PA6 and PA6-CNT/G systems (Dharmawardhana et al. 2017; Heinz et al. 2013); IFF was also used to predict bulk modulus. The recently developed IFF-R was used for the uniaxial and shear deformation simulations used in predicting Young's and shear moduli, and Poisson's ratio (Heinz 2021; Winetrout et al. 2021; Odegard et al. 2021; Pisani et al. 2021b). IFF-R incorporates the Morse potential for fast, accurate bond scission capabilities useful for large deformations.

The various LAMMPS force field styles were set as follows. The class 2 style was set for bonds, angles, dihedrals, and impropers. The atom style was set to full (bonds, angles, dihedrals, impropers, and partial charges). The pair mixing style was set to sixth power. The weighting coefficients for non-bonded Lennard-Jones and Coulombic interactions were specified such that non-bonded interactions were turned off for atoms directly bonded to each other and atoms one bond away. However, atoms two bonds away experience non-bonded interactions at full force. The "lj/class2/coul/cut" pair style was used for the densification step; the Coulombic Lennard-Jones cutoff was set to 10 Å. After densification, long-range dispersion forces were included via the "lj/class2/coul/long" pair style; the Coulombic Lennard-Jones cutoff remained set at 10 Å. The kspace solver was PPPM[1]; the relative accuracy of the kspace solver was set to 1×10^{-6}. For the uniaxial tensile and shear simulations, the bond style was set to hybrid with class 2 and Morse; bonds with equilibrium bond distances longer than or equal to 1.40 Å were converted into Morse bonds via an in-house conversion tool.

[1] particle-particle particle-mesh

2.1.2 Neat PA6

The PA6 monomer as used in this work is shown in Figure 1. An in-house Python and BASH tool was used to generate the initial PA6 structure with IFF parameters. Three neat amorphous PA6 systems were established in IFF for the PA6-CNT/G simulations. These three systems were reused for the multiscale modeling; however, to satisfy reviewers of the multiscale modeling manuscript, five more neat amorphous PA6 systems were established in IFF for a total of eight neat amorphous PA6 systems. Each system initially contained 25,168 atoms (1,144 PA6 monomers). Each system was densified from the initial gaseous state to the bulk density of amorphous PA6 (1.084 g cm^{-3}) at a rate of 20 Å ns^{-1}; the NVT (N is constant number of particles, V is constant volume, T is constant temperature) ensemble at 300 K was used. After densification, the PA6 replicates were polymerized via the LAMMPS command "fix bond/react" (Gissinger et al. 2017) at 300 K and 1.0 atmospheres (atm) using NPT (N is constant number of particles, P is constant pressure, T is constant temperature) ("aniso" keyword). PA6 undergoes a linear polycondensation reaction: in Figure 1, the nitrogen (10) bonds with the carbon (3), and a water molecule is produced (1-2-21). A polymerization conversion of 90% was targeted for computational efficiency; a higher polymerization would require significantly more simulation time due to a rapidly diminishing return on new bonds. The initial three replicates were polymerized for a fixed time of 600 picoseconds (ps). The five additional replicates were polymerized in 1000-step increments until they reached 90% conversion; the average simulation time was 545 ps.

The specific "fix bond/react" parameters used are as follows. The "stabilization" keyword was used to stabilize each reaction site with a “fix nve/limit” (N is constant number of particles, V is constant volume, E is constant energy) time integrator for 500 time-steps. The stabilized atoms were prevented from moving more than 0.03 Å per time-step. The reaction was set to occur every 100 time-steps with a probability of 0.001. The minimum distance was set to 0 Å, and the maximum distance was set to 7 Å. The "update_edges" keyword with the parameter "charges" was used to update the charges of edge atoms specified by the post-reaction template. This prevented the system from becoming charged (which is undesirable when including long-range Coulombic interactions). To prevent reacting atoms from destabilizing the system, the “fix temp/rescale” command was used to rescale their temperature to 300 K at every time-step when their temperature was more than 10 K away from 300 K. The produced water

molecules were immediately deleted after forming, using the deleteIDs keyword in the mapping file to simulate a fully dried material.

After polymerization, the neat PA6 systems were equilibrated for 2 nanoseconds (ns) at 300 K and 1.0 atm using NPT ("aniso keyword") to allow the systems to relax and reduce residual stresses. A snapshot of one of the final equilibrated, polymerized PA6 MD models is shown in Figure 2. During equilibration, time-averaged stresses (here considered to be residual stresses) in the *x*-, *y*-, and *z*-directions were taken every 1000 time-steps and logged. These residual stresses were then plotted as a function of time. If the residual stresses fluctuate about zero, then residual stresses are confirmed to be negligible. All eight systems' residual stresses were confirmed to be negligible. Prior to simulating shear and uniaxial strain, class 2 bonds with an equilibrium bond length of 1.40 Å or greater were converted to Morse bonds using an in-house tool. Each equilibrated, polymerized PA6 system was strained uniaxially in the *x*-, *y*-, and *z*-directions for a total of 24 uniaxial tension simulations (eight replicates multiplied by three uniaxial tensile simulations). Similarly, the PA6 systems were sheared in the *xy*-, *xz*-, and *yz*-directions for a total of 24 shear simulations. The amorphous PA6 systems were assumed to be isotropic thus allowing for the results of the shear and uniaxial tension simulations to be averaged together. For both the shear and uniaxial tensile simulations, the "fix deform" command was used to apply a 2×10^8 s^{-1} strain rate over 1 ns resulting in a 20% engineering strain. The NPT ensemble was used to set the temperature to 300 K and set the pressure in the directions transverse to the strain to 1 atm to allow for Poisson contractions.

An in-house R tool using the "Segmented" package (Muggeo 2003) was used to compute the elastic moduli from the stress-strain curves by fitting a series of segmented regressions to the curves.

The elastic moduli were assumed to be the slope of the first segmented regression of their respective stress-strain curves. The predicted elastic moduli of the amorphous PA6 systems (n = 8) are as follows: Young's modulus = 1.80 ± 0.38 GPa; Poisson's ratio = 0.39 ± 0.08; and shear modulus = 0.59 ± 0.08 GPa.

Figure 1. PA6 monomer as used in this work. Marvin was used to create the chemical structure in this figure, Marvin 21.10, ChemAxon (https://www.chemaxon.com).

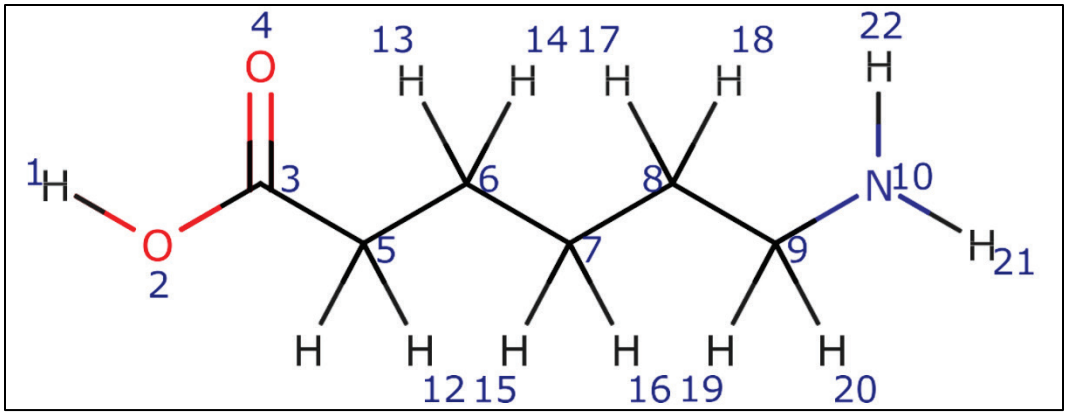

Figure 2. Equilibrated, polymerized PA6 MD model. Colors follow the Corey-Pauling-Koltun (CPK) coloring convention.

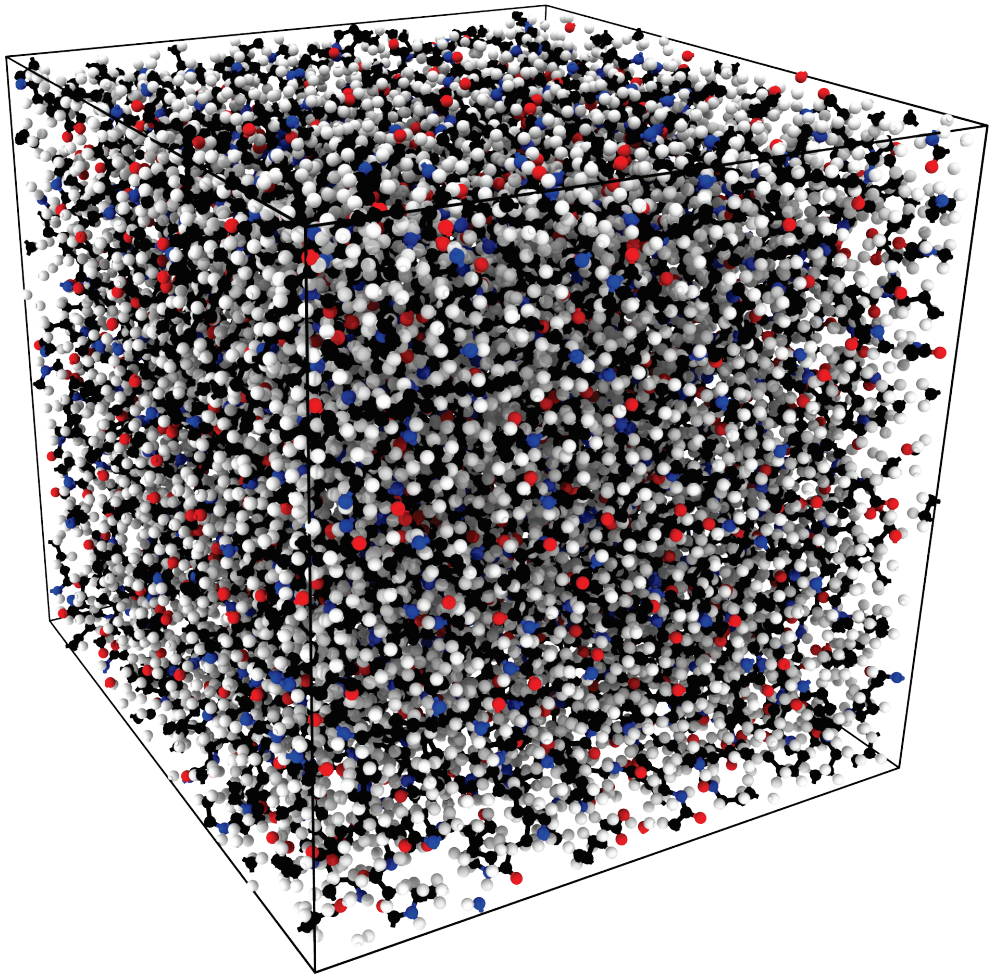

2.1.3 Carbon nanotube and graphene

A capped (6,6) 35.6 Å long CNT was generated by JCrystalSoft's Nanotube Modeler (http://www.jcrystal.com/products/wincnt/) as an xyz coordinate file. An in-house Python script was used to transform the xyz file into an IFF LAMMPS data file with bonds, angles, dihedrals, and impropers, as well as the appropriate force field parameters and to attach two virtual π electrons to each CNT atom and add the corresponding bond, angle, and dihedral information. The CNT was minimized (Polak-Ribiere conjugate gradient algorithm, energy tolerance of $1.0e^{-5}$, force tolerance of $1.0e^{-7}$, maximum iterations at 1,000, and maximum number of force/energy evaluations at 10,000), run at 300 K for 200 ps (NVT, and then equilibrated at 300 K and 1 atm for 1 ns (NPT aniso). The "fix momentum" command was invoked every 100 time-steps to prevent the CNT from drifting during both the NVT and NPT runs. The equilibrated structure (Figure 3) was then ready to combine with PA6 molecules.

A 30.59 Å × 11.99 Å hydrogen-terminated graphene sheet was generated using a combination of LAMMPS and an in-house Python script. LAMMPS was used to generate the G atoms in a hexagonal lattice; the Python script was used to create bonds, angles, dihedrals, virtual π electrons, and terminal-hydrogen atoms, as well as the IFF parameters. The resulting G data file contains the virtual π electrons as well as hydrogen atoms terminating the edges of the G sheet (Figure 3). The G sheet was not simulated prior to combination with the PA6 monomers due to its smaller size (414 atoms) compared to the CNT (1044 atoms).

Figure 3. The capped (6,6) 30 Å long CNT and 30.59 Å x 11.99 Å hydrogen-terminated G sheet as used in this work. Two virtual π electrons are bonded to each carbon atom for enhanced Coulombic interactions. Colors follow the CPK convention; the virtual π electrons are colored light-purple (HTML: f847de2).

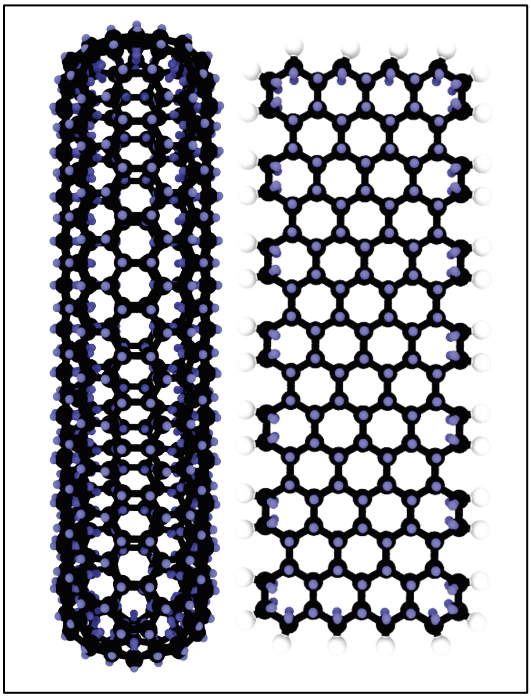

2.1.4 PA6-CNT/G nanocomposites

The mass fractions of CNT/G in the PA6 nanocomposites ranged from 0 to 0.08 in 0.01 increments. Each mass fraction had three replicates for statistical analysis, and each system contained two CNTs or two G sheets. The PA6/CNT system sizes range from 160,928 atoms (1% CNT) to 20,568 atoms (8% CNT); the PA6/G system sizes range from 59,634 atoms (1% G) to 7,670 atoms (8% G).

The combination procedure used to combine the CNTs and G with PA6 monomers is detailed as follows. First, the PA6 monomer was read into LAMMPS and then replicated the required number of times in the *x*-, *y*-, and *z*-directions to achieve the specified mass fraction reinforcement after 90% polymerization. Second, the simulation box dimensions were reset so that the origin was (0,0,0); the atoms were remapped to fit into this new box. Third, the CNT/G data file was read in twice ("read_data append" command), with each set of atoms assigned to a different group. Fourth, the simulation box dimensions were reset once more so that the origin was

(0,0,0) and the atoms remapped. Fifth, the simulation box was enlarged by 80 Å in the *x*- and *y*-dimensions; the atoms were not remapped so that the empty space remained. The CNTs/G were then moved into this empty region in different directions via the "displace_atoms" command. One CNT/G was moved only in the *x*-direction and the other CNT/G was moved only in the *y*-direction. The distance displaced from (0,0,0) was dependent on the size of the simulation in the dimension displaced. This was done to prevent PA6 molecules from getting stuck in the CNTs/G.

Now combined, the atoms were given velocities corresponding to a temperature of 300 K; each sample was given a different velocity seed to ensure different results. The systems were then minimized with the Polak-Ribiere conjugate gradient algorithm (energy tolerance of 1.0e^{-5}, force tolerance of 1.0e^{-7}, maximum iterations at 1,000, and maximum number of force/energy evaluations at 10,000). The systems were then densified to a density determined using an inverse rule of mixtures relationship shown in Equation 1 (Pisani 2021a).

$$l = \left(10^{24} M \left(\frac{m_{filler}}{\rho_{filler}} + \frac{1-m_{filler}}{\rho_{PA6}}\right)\right)^{1/3} \quad (1)$$

ρ_{filler} is the density of CNT/G at 1.8 g cm^{-3}/2.23 g cm^{-3}, ρ_{PA6} is the density of the polymer system (1.084 g cm^{-3} for nylon 6), M is the total mass of the system in g, 10^{24} is a conversion factor, m_{filler} is the mass fraction of CNT/G, and l is the length of each side of the simulation box in Å required to achieve the density.

The systems were densified in two stages: the first was a fast densification (300 Å ns^{-1}, to save computational resources) to a density 1.25 times the target density; the second was a slower densification (25 Å ns^{-1}, ensuring that molecules were not forced into unnatural conformations) to the target density. The "fix deform" command was used to densify the simulation box. The NVT ensemble at 300 K was used. During the first stage, the boundary conditions were set to fixed in *x*-, *y*-, and *z*-directions. The "fix wall/reflect" command was used to set up reflective walls at the boundaries; this was done to help prevent the CNTs/G from encountering each other early in the MD construction process. The "fix deform" command was invoked at each time-step to shrink the simulation box to the target density. At the end of the first stage, the boundaries were changed back to periodic in each direction, and the atoms were remapped.

After densification, long-range Coulombic interactions were enabled with a Lennard-Jones and Coulombic cutoff of 10.0 Å, and then each system was annealed to increase the mobility of the Nylon 6 molecules and allow them to achieve a more desirable configuration. The temperature was ramped to 400 K (approximately 80 K higher than the glass transition temperature of PA6) over 100 ps using NVT. The temperature was then decreased by 25 K ns^{-1} to 300 K. After annealing, the CNT/G nanocomposites were equilibrated at 300 K and 1.0 atm with NPT aniso/iso for 4/2 ns to relax the systems and reduce residual stresses. The PA6-CNT models were equilibrated for twice as much time as the PA6-G models because the PA6-CNT models are significantly larger.

After equilibration and in parallel with the polymerization simulations, the bulk modulus of the unpolymerized systems was predicted by holding the pressure constant at 1.0 atm for 500 ps and then holding the pressure constant at 5000.0 atm for another 500 ps. The average pressure and volume at the 1.0 atm stage and the 5000.0 atm stage as well as the initial volume at the first stage were used to compute bulk modulus according to the equation $K = -\frac{\Delta P}{\Delta V/V}$.

The equilibrated nanocomposites were polymerized using the "fix bond/react" command in LAMMPS (Gisenger et al. 2017). The systems were polymerized with the same "fix bond/react" settings as the neat PA6 systems but were run with NPT aniso at 300 K and 1.0 atm for 600 ps; the runtime was chosen to produce systems with approximately 90% polymerization. After polymerization, each replicate was annealed and equilibrated using the same methodology as before polymerization (see Figure 4 for example images of the equilibrated, polymerized MD models). An explicit check for residual stresses was conducted on the polymerized, equilibrated nanocomposites; residual stresses were negligible. The bulk modulus was predicted for the polymerized, equilibrated nanocomposites using the same methodology as before.

In addition to predicting bulk modulus, the Young's modulus of each polymerized replicate was also computed. Each nanocomposite replicate was subjected to uniaxial tensile strains along the *x*-, *y*-, and *z*-axes. The "fix deform" command was used to apply a 2×10^8 s^{-1} strain rate over 1 ns resulting in a 20% engineering strain. The temperature of the system was set to 300 K; the pressure in the transverse directions was set to 1 atm to allow for Poisson contractions (NPT ensemble). The stress-strain curves

from the uniaxial tensile simulations were analyzed with the same in-house R-script as the neat PA6 MD models to obtain Young's modulus.

Figure 4. Example images of equilibrated, polymerized PA6-CNT (top-left) and PA6-G (top- right) MD models. The bottom images show the distribution of the CNT and G molecules within the example models by removing the polymer matrix. Colors follow the CPK convention; the virtual π electrons are colored light purple (HTML: f847de2).

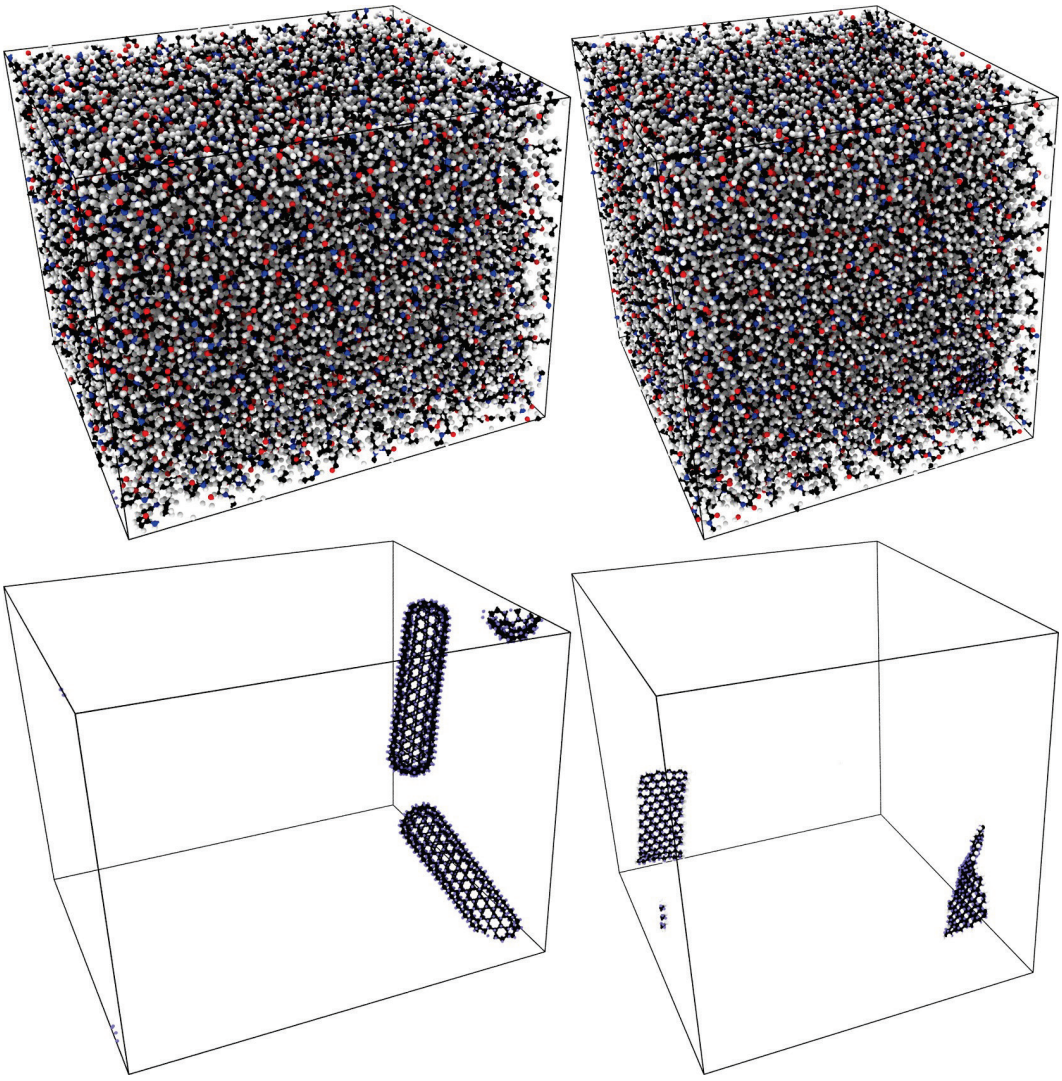

2.2 Multiscale modeling

The NASA Glenn Research Center's MAC/GMC was used for the multiscale modeling in this report. Specifically, the MSGMC module of MAC/GMC was used for the computation of the mechanical properties of the multiscale model presented in this study. The mathematical theory behind MAC/GMC and MSGMC can be found elsewhere (Pisani et al. 2019; Aboudi et al. 2013, 984; Aboudi et al. 2021, 416). MAC/GMC has

quite recently been succeeded by NASA Multiscale Analysis Tool (NASMAT) (Pineda et al 2021).

A complete description of the multiscale model may be found in the introductory paper (Pisani et al. 2019), but an abridged description is included here for ease of use. Figure 5 shows the multiscale model as used in this work. Levels 2, 3, and 4 in Figure 5 are close to identical to the multiscale model in the previous paper (Pisani et al. 2019). Level 1 is actually also in the code of the previous version of the multiscale model, but it is made explicit here in Figure 5. The multiscale model spans four length scales with five levels; the superscripts on the axes refer to the level while the subscripts refer to the coordinate axis. Level 0 consists of the MD-predicted mechanical properties of amorphous PA6 and the stiffness matrices of the α and γ PA6 crystal forms as computed by Tashiro and Tadokoro (see Equations 2 and 3) (Tashiro and Tadokoro 1981). The amorphous PA6 MD predictions were used as input into Level 2 while the stiffness matrices were used as input into Level 1; the predicted elastic moduli of the amorphous PA6 systems (n = 8) are as follows: Young's modulus = 1.80 ± 0.38 GPa; Poisson's ratio = 0.39 ± 0.08; and shear modulus = 0.59 ± 0.08 GPa. Level 1 was used to easily change the orientation of the stiffness matrices of the crystals relative to Level 2. Despite the isotropy of the spherulite, changing the orientation of the dummy crystal relative to the crystallite changes the resulting spherulite properties slightly. A sweep of the orientations as a function of crystallinity was performed to determine the most appropriate orientation for the study. The orientation as seen in Level 1 of Figure 5 was chosen because the mechanical properties were close to being an average of all orientation results. In this optimal orientation Level 1 axis 1 is aligned with Level 2 axis 2, Level 1 axis 2 is aligned with Level 2 axis 1, and Level 1 axis 3 is aligned with Level 2 axis 3.

$$C_{\alpha} = \begin{bmatrix} 12.44 & 2.68 & 2.00 & 0 & 0 & 4.40 \\ 2.68 & 5.20 & 0.75 & 0 & 0 & 0.82 \\ 2.00 & 0.75 & 312.33 & 0 & 0 & 0.06 \\ 0 & 0 & 0 & 2.33 & -0.39 & 0 \\ 0 & 0 & 0 & -0.39 & 0.95 & 0 \\ 4.40 & 0.82 & 0.06 & 0 & 0 & 3.65 \end{bmatrix} GPa \qquad (2)$$

$$C_\gamma = \begin{bmatrix} 5.27 & 1.77 & 0.80 & 0 & 0 & -0.96 \\ 1.77 & 17.52 & 4.47 & 0 & 0 & 0.67 \\ 0.80 & 4.47 & 54.96 & 0 & 0 & -0.44 \\ 0 & 0 & 0 & 4.44 & -0.63 & 0 \\ 0 & 0 & 0 & -0.63 & 2.35 & 0 \\ -0.96 & 0.67 & -0.44 & 0 & 0 & 2.75 \end{bmatrix} GPa \quad (3)$$

The dummy crystal at Level 1 is a 1 × 1 doubly periodic repeating unit cell (RUC) but is portrayed in 3D in Figure 5. Level 1 is inserted into the lavender-colored regions of Level 2, and the alignment of Level 1 relative to Level 2 is shown in Figure 5. The PA6 crystallite at Level 2 is a 5 × 5 doubly-periodic RUC. The PA6 crystallite was based on the inner four blue subcells and the immediate red amorphous surroundings of the granular crystal block structure in the PEEK microstructure schematic by Wang et al. (2016). The crystallinity of Level 2 was set to 86.2% to match the crystallinity of the experimental granular crystal block structure as reported by Wang et al. (2016). The plank with amorphous PA6 structure at Level 3 is a 2 × 2 doubly periodic RUC and corresponds to the lamellae stacks structure in the PEEK microstructure schematic by Wang et al. (2016). The PA6 crystallite from Level 2 is inserted into one of the four subcells (Level 2 axis 1 is aligned with Level 3 axis 1, Level 2 axis 2 is aligned with Level 3 axis 2, and Level 2 axis 3 is aligned with Level 3 axis 3) while the remaining three subcells are given the MD-predicted mechanical properties of amorphous PA6. The overall crystallinity of Level 2 can be adjusted by changing the internal subcell dimensions of the RUC. Allowing the crystallinity of Level 3 to change allows the multiscale model to predict mechanical properties of semi-crystalline PA6 as a function of crystallinity. The spherulite RUC at Level 4 is a 6 × 6 × 6 triply periodic RUC and corresponds to the spherulite. Note that the spherulite RUC was chosen to be representative of bulk semi-crystalline PA6; the root network was not modeled. Each subcell of the spherulite RUC is a plank with amorphous PA6 RUC, but each subcell is oriented differently, and the crystallinity can change. The experimental spherulite is more crystalline-dense in the center of the structure and less-so as the distance from the center increases. Level 4 captures this crystallinity distribution by decreasing the crystallinity of the subcells as the distance from the center of the spherulite RUC increases. Note that each subcell in Level 4 is oriented using three vectors. The first vector is oriented pointing from the center of the overall spherulite to the center of the subcell. This mimics the radial nature of the spherulite. The other two vectors are orthogonal to the first and are randomly generated at runtime. A Python program was

written to construct the multiscale model and write the MAC/GMC input file, run MAC/GMC, and collect and average the predicted mechanical properties. The random generation of the two vectors results in slight deviations from perfect isotropy; the results of 75 individual runs were averaged together to account for these deviations. The amorphous PA6 MD mechanical properties of each run are drawn from a uniform distribution spanning one standard deviation away from the average in both positive and negative directions and then input into the multiscale model. The stiffness matrices of the α and γ crystal forms do not have standard deviations and thus stay the same run to run.

Figure 5. The multiscale model as used in this work.

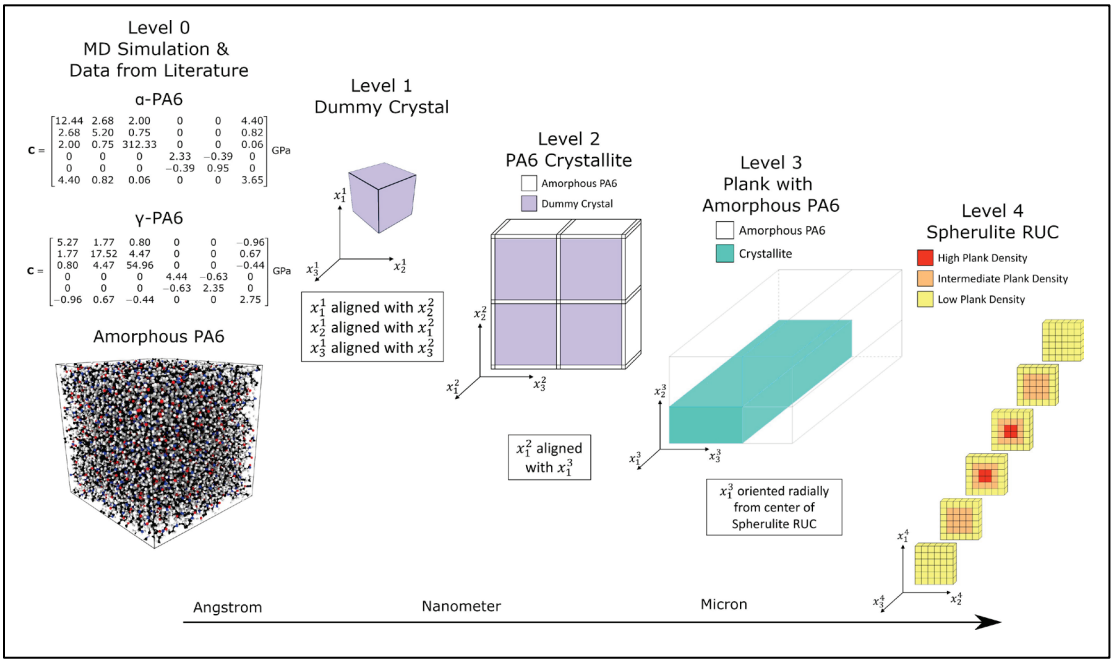

2.3 Experimental methods

2.3.1 Materials

Nylon 6 (PA6) was purchased from Scientific Polymer Products and used as received. M-cresol (99%) and 2-propanol were purchased from Fisher Scientific and used as received for solvent casting and film delamination respectively. Single-/double-walled CNTs and graphene nanoplatelets (GNPs) were purchased from Cheaptubes.com. CNTs had an average outer diameter of 1–4 nm and a length of 0.5–2.0 μm. GNPs had an average thickness of 8–15 nm and a length of 2 μm.

2.3.2 Film preparation

PA6 was dissolved in m-cresol to create a 10 wt% solution in a wide-mouthed flat-bottom flask. An overhead stirrer was used to dissolve the PA6 at a speed of 300 rpm overnight. A portion of this master batch was taken out and placed into a mixing cup along with the desired wt% loading of CNT or GNP. These mixtures were high shear mixed for two 5 min cycles at 3,500 rpm, resting between each cycle for 5 min. Films were cast onto glass panels and placed in an oven at 100°C overnight to remove residual solvent. The cast glass panels were soaked in 2-propanol for 30 min to delaminate the film. Free-films were placed back in oven at 60°C to ensure removal of 2-propanol before evaluation.

2.3.3 Mechanical testing

Thin-film (0.02–0.09 mm thickness) composites were cut into 6 × 15 mm strips along the draw direction and characterized using a TA Instruments RSA-G2 solids analyzer in the tension test fixture. Samples were evaluated at 25°C at a constant linear rate of 0.01 mm/min, with a loading gap of 50 mm. Young's modulus was subsequently calculated from the generated stress vs. strain curve.

3 Results and Discussion

3.1 PA6-CNT/G mechanical properties

Figure 6 shows bulk modulus as a function of CNT/G loading for the polymerized CNT and G nanocomposites. It appears that the addition of CNT/G does not significantly change the predicted bulk modulus as the CNT/G loading increases. Perhaps the reinforcing effect would be different in the presence of PA6 crystals. There is generally a relationship between the strength of the interface and load transfer from matrix to reinforcement. It is interesting that the PA6-G systems have similar bulk moduli predictions as the PA6-CNT even though the G reinforcement has, on average, 68% stronger interaction energy with the PA6 matrix than the CNT reinforcement. With the significantly stronger interaction energy, it was expected that the PA6-G systems would have significantly greater bulk moduli than the PA6-CNT systems. It is possible that the capped CNTs respond to isotropic compression significantly better than the G sheets, so despite the higher interaction energy of the PA6-G systems, the bulk moduli of the PA6-CNT systems are similar to that of the PA6-G systems.

Figure 6. Bulk modulus of the polymerized PA6-CNT and PA6-G nanocomposites as a function of target mass fraction reinforcement. The Neat and PA6-CNT *x*-values have been shifted right slightly to provide a clearer comparison.

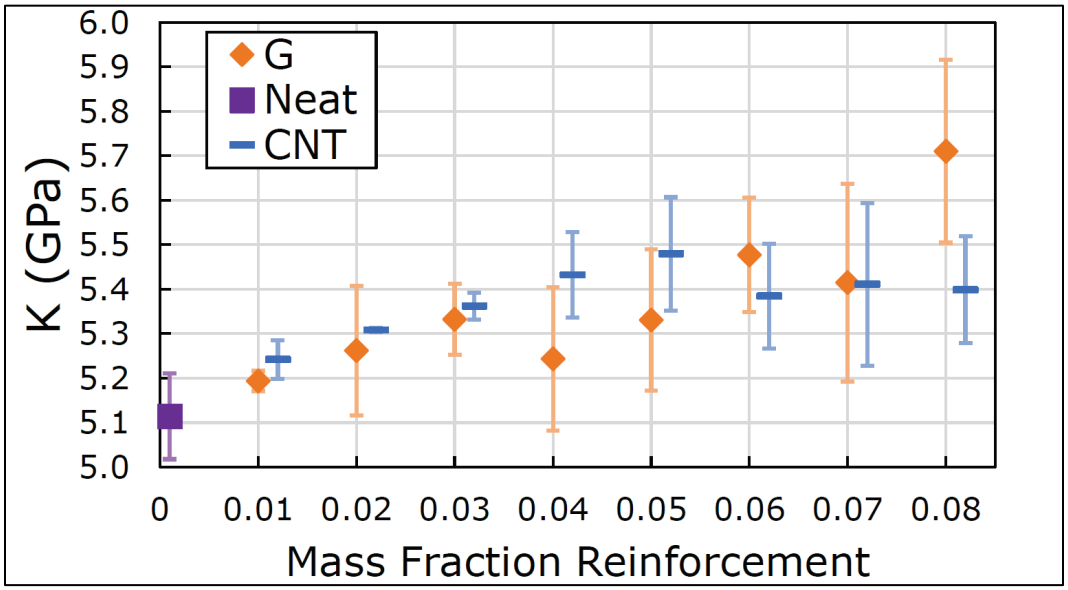

The reinforcing effect of CNTs and Gs on amorphous PA6 with regards to Young's modulus appears to be relatively small as shown in Figure 7. Perhaps the reinforcing effect of CNT/G would be different in the presence of crystallinity. The relatively small improvement in Young's modulus as predicted by the authors' computations is in line with earlier results where Faghihi et al. (2105) reported a similar trend for PA6-CNT composites. The largest increases in Young's modulus occur at 4 wt% G and 5 wt% CNT, which are 14% and 15% higher than neat PA6, respectively.

Figure 8 shows a comparison of predicted and experimental values of Young's modulus for neat PA6, PA6-CNT, and PA6-G systems. As there are only experimental data for 0 to 4 wt% CNT/G, only those MD predictions are shown in Figure 8. There is mixed agreement between the experimental data and MD predictions. Most of the experimental values do not match well with the predictions; in these cases, the MD predictions are nearly double that of the experimental values. The reason for the discrepancies appears to be agglomeration of CNTs and GNPs in the experimental samples. Agglomeration is known to have significant negative effects on the mechanical properties of polymer composites. The MD systems had little to no agglomeration.

Figure 7. Comparison of predicted Young's modulus as a function of mass fraction reinforcement between neat PA6, PA6-CNT, and PA6-G. The neat PA6 and PA6-CNT values are offset slightly for clarity.

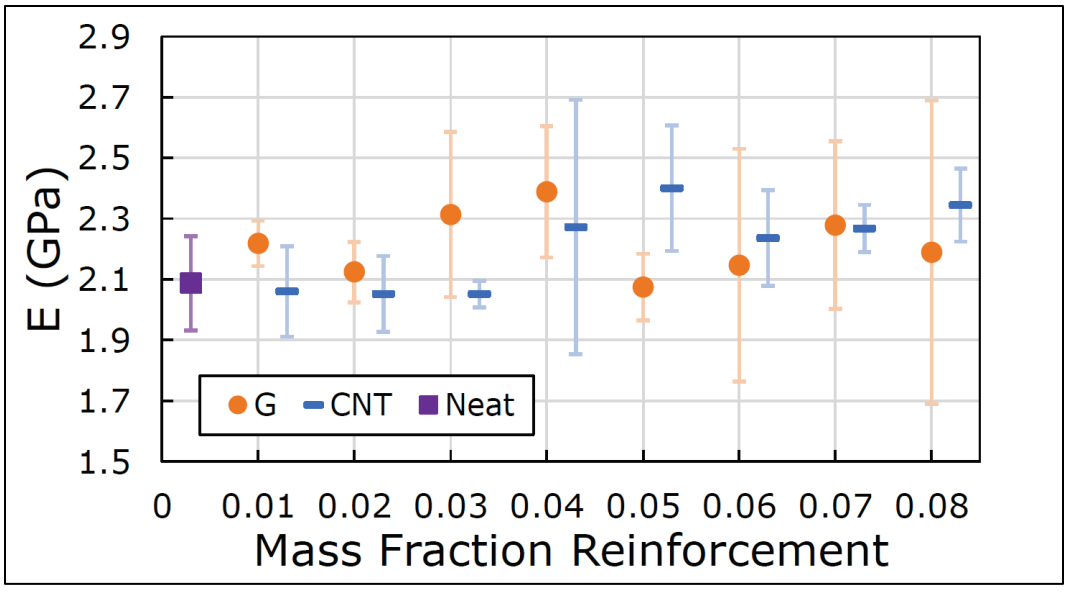

Figure 8. Comparison of predicted and experimental Young's modulus as a function of mass fraction reinforcement between neat PA6, PA6-CNT, and PA6-G. Only the MD mass fractions which have experimental data are shown. The neat PA6, PA6-CNT, and literature values are offset slightly for clarity.

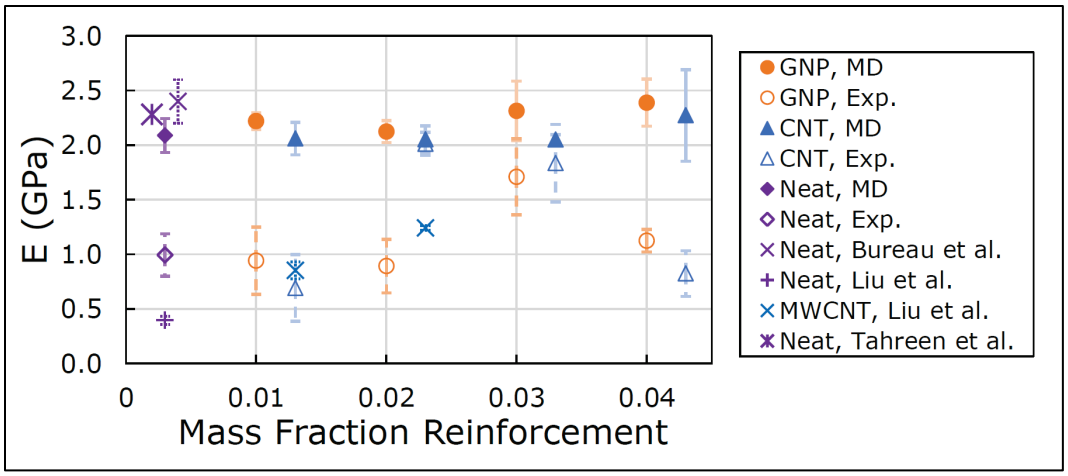

3.2 Multiscale modeling results

The multiscale modeling predictions as a function of α and γ crystallinity are shown in Figures 9 (Young's modulus), 10 (shear modulus), and 11 (Poisson's ratio). This multiscale model can predict mechanical properties as a function of crystallinity up to 75% crystalline, which is greater than neat PA6's maximum experimentally achievable crystallinity of 60% (Huang et al. 2011) This enables a better understanding of the trends.

Figure 9 shows the predicted Young's modulus as a function of α and γ crystallinity. From 0% to 40% crystallinity, there is not a significant difference between the α and γ crystal forms. However, the difference between the Young's modulus of the two crystal forms increases as the crystallinity increases past 40%; the γ-form has higher Young's modulus values than the α-form. This phenomenon is present in the shear modulus predictions as well (Figure 10); the γ-form has higher shear modulus values than the α-form. The orientations/alignments of each level of the multiscale model relative to each other are the reason for the γ-form having greater Young's and shear moduli than the α-form. As shown in the α/γ stiffness matrices (Equations 2 and 3), the α-form has a significantly higher axial stiffness (C33) than the γ-form. However, due to the rotation of the stiffness matrices within the multiscale model, this axial stiffness does not end up aligning with the radial direction of the spherulite (which is the direction primarily responsible for the mechanical properties of the spherulite). The stiffness aligned with this radial direction (the axial

direction of the plank) is a magnitude larger in the γ-form (≈12 GPa) than in the α-form (≈ 4 GPa), and thus are the reason for the γ spherulites having higher Young's moduli than the α spherulites. Similarly, the greater radial shear moduli of the γ-form at the plank level are the reason for the higher shear moduli of the γ-spherulites.

In Figure 9, the predicted Young's modulus values compare well with most of the literature values. It is possible that the degree of increase in the Young's modulus as the crystallinity increases is greater than the multiscale model predicts. That is, the experimental results of Bureau et al. (2002) and da Paz et al. (2016) suggest that the Young's modulus increases at a lower degree of crystallinity than this model shows. However, it is impossible to know for certain without more experimental data, especially mechanical property data of high crystallinity. Overall, the good agreement between the multiscale model predictions and most of the literature values of Young's and shear moduli validate the use of this multiscale model for prediction of Young's and shear moduli as a function of crystallinity for semi-crystalline PA6. In Figure 11, the Poisson's ratio decreases with an increase in crystallinity, which agrees with experimental trends that Poisson's ratio typically decreases with an increase in Young's and shear moduli. The wide range of the error bars shows that there is not a significant difference between the α and γ Poisson's ratios. Validation of the predicted Poisson's ratio data was not possible due to a lack of experimental data.

Figure 9. Predicted effect of α and γ crystallinity on Young's modulus; predictions are delineated with dashed lines. Experimental (Bureau et al. 2002; da Paz et al. 2016; Faghihi et al. 2015; Designer Data 2021) and simulation (Huang et al. 2011) data from literature are included for comparison.

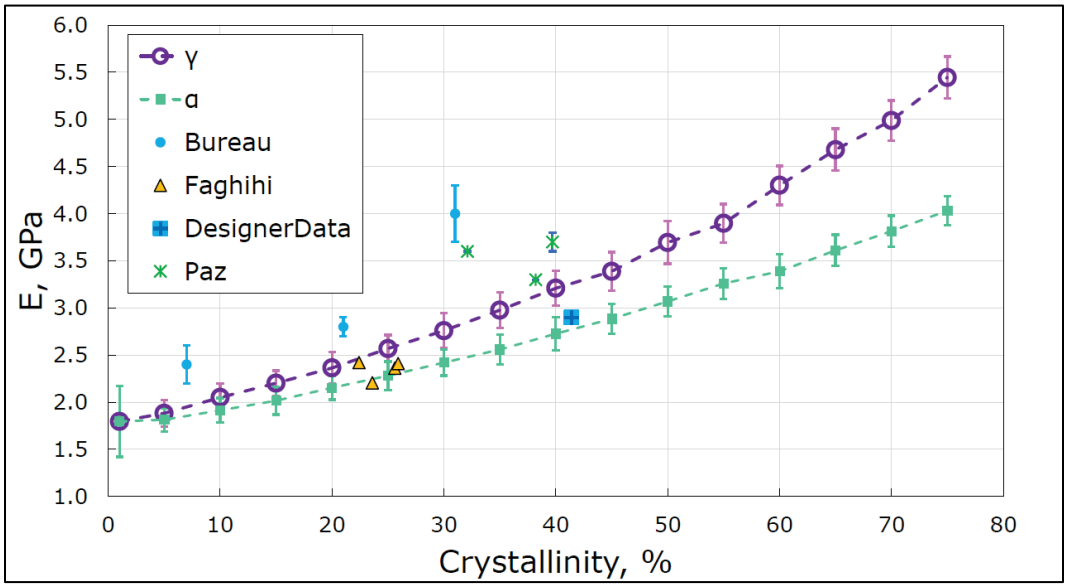

Figure 10. Predicted effect of α and γ crystallinity on shear modulus; predictions are delineated with dashed lines. Data from literature are included for comparison (Shibukawa et al. 1962).

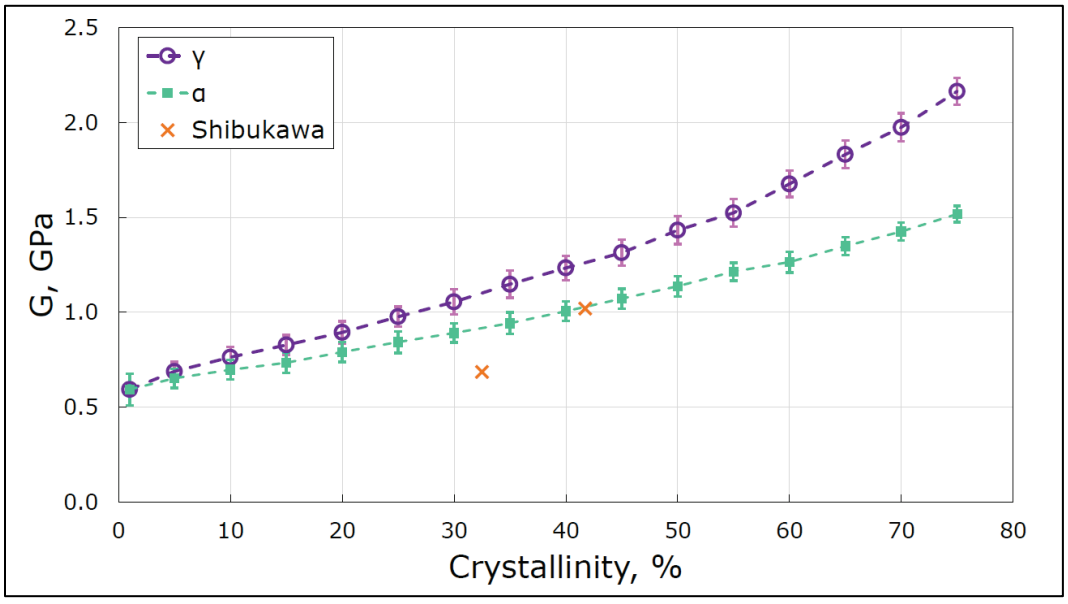

Figure 11. Predicted effect of α and γ crystallinity on Poisson's ratio.

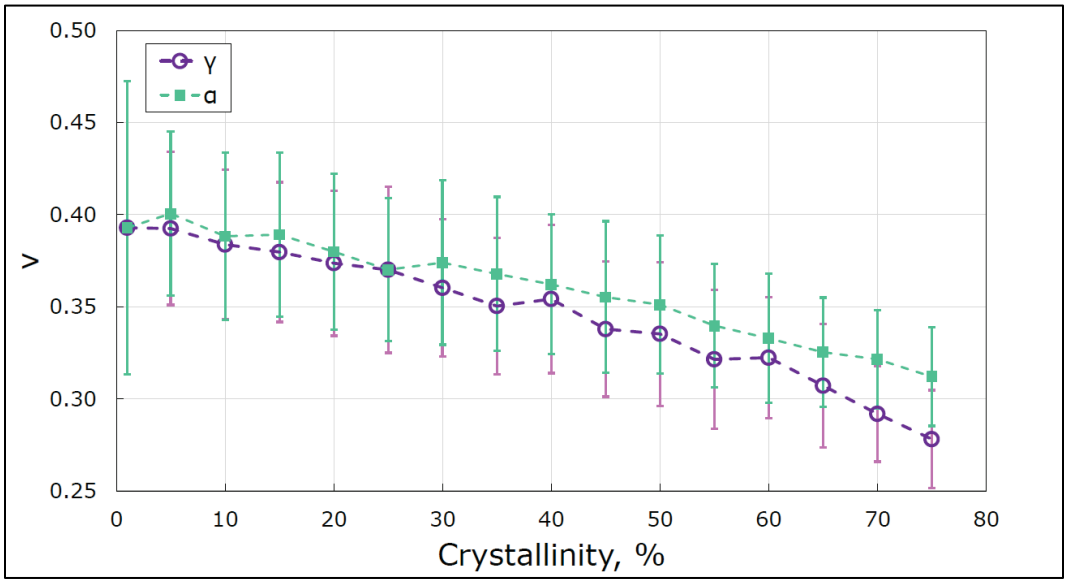

4 Conclusions

In this study, two structure-property relationships of PA6 were explored via MD simulation and multiscale modeling: (1) the effect of CNT/G on mechanical properties of amorphous PA6 and (2) the effect of crystallinity and crystal form on mechanical properties of semi-crystalline PA6. MD simulations with the IFF and IFF-R were used to construct (IFF) and predict mechanical properties (IFF-R) of the neat amorphous PA6 and the amorphous PA6-CNT/G systems.

1. MD simulation was used to predict bulk and Young's moduli of amorphous PA6-CNT/G nanocomposites as a function of CNT/G loading. The bulk modulus of the amorphous PA6-CNT/G nanocomposites is not significantly improved by the addition of up to 8 wt% CNT/G; perhaps the reinforcing effect of CNTs/G would be different in the presence of PA6 crystals. The mechanical property predictions for both PA6-CNT and PA6-G nanocomposites were largely similar for both bulk and Young's modulus despite a significantly greater interaction per atom between G and PA6 matrix. The predicted values of Young's modulus agree moderately well with the experimental values.
2. A multiscale modeling approach was used to predict mechanical properties as a function of crystallinity and crystal form (α/γ) of semi-crystalline PA6. NASA Glenn Research Center's micromechanics software MAC/GMC was used to facilitate the multiscale modeling. The inputs to the multiscale model were the elastic moduli of amorphous PA6 as predicted via MD and calculated stiffness matrices from the literature of the PA6 α and γ crystal forms. The multiscale model output was Young's modulus, shear modulus, and Poisson's ratio as a function of α and γ crystallinity. The predicted values of Young's modulus and shear modulus compared well with experiment. The multiscale model predictions showed that the mechanical properties of semi-crystalline PA6 with α and γ crystal forms are similar for amorphous to 40% crystalline, and diverge after this limit, with the γ PA6 predictions having higher Young's and shear moduli and lower Poisson's ratio.

References

Aboudi, J., S. M. Arnold, and B. A. Bednarcyk. 2013. *Micromechanics of Composite Materials: A Generalized Multiscale Analysis Approach*. Amsterdam, Netherlands: Elsevier.

Aboudi, J., S. M. Arnold, and B. A. Bednarcyk. 2021. *Practical Micromechanics of Composite Materials,* 1st ed. Oxford, UK: Butterworth-Heinemann.

Al Mahmud, H., M. S. Radue, S. Chinkanjanarot, W. A. Pisani, S. Gowtham, and G. M. Odegard. 2019. "Multiscale Modeling of Carbon Fiber-Graphene Nanoplatelet-Epoxy Hybrid Composites Using a Reactive Force Field." *Compos. Part B Eng*. 972:628–635.

Bednarcyk, B. A., and S. M. Arnold. 2002. *MAC/GMC 4.0 User's Manual - Keywords Manual*. NASA/TM—2002-292077/Vol2.

Bureau, M. N., J. Denault, K. C. Cole, and G. D. Enright. 2002. "The Role of Crystallinity and Reinforcement in the Mechanical Behavior of Polyamide-6/Clay Nanocomposites." *Polym. Eng. Sci.* 42:1897–1906.

Chinkanjanarot, S., M. S. Radue, S. Gowtham, J. M. Tomasi, D. R. Klimek-McDonald, J. A. King, and G. M. Odegard. 2018. "Multiscale Thermal Modeling of Cured Cycloaliphatic Epoxy/Carbon Fiber Composites." *Journal of Applied Polymer Science* 135:46371.

Cross, D. R., K. T. Tan, E. J. Pineda, B. A. Bednarcyk, and S. M. Arnold. 2018. "Multiscale Modeling of Carbon Fiber-Reinforced Polymer Composites in Low-Temperature Arctic Conditions." *Multiscale and Multidisciplinary , Modeling, Experiments and Design* 9:239–254.

da Paz, R. A., A. M. D. Leite, E. M. Araujo, V. d. N. Medeiros, T. J. A. de Melo, and L. A. Pessan. 2016. "Mechanical and Thermomechanical Properties of Polyamide 6/Brazilian Organoclay Nanocomposites." *Pol meros* 26:52–60.

DesignerData. PA6. n.d. Accessed 2021-08-18. https://designerdata.nl/materials/plastics/thermo-plastics/polyamide-6.

Dharmawardhana, C. C., K. Kanhaiya, T.-J. Lin, A. Garley, M. R. Knecht, J. Zhou, J. Miao, and H. Heinz. 2017. "Reliable Computational Design of Biological-Inorganic Materials to the Large Nanometer Scale Using Interface-FF." *Mol. Simul.* 4:1394–1405.

Faghihi, M., A. Shojaei, and R. Bagheri. 2015. "Characterization of Polyamide 6/Carbon Nanotube Composites Prepared by Melt Mixing-Effect of Matrix Molecular Weight and Structure." *Compos. Part B Eng*. 7:50–64.

Fornes, T. D., and D. R. Paul. 2003. "Crystallization Behavior of Nylon 6 Nanocomposites." *Polymer* 44:3945–3961.

Fu, X., C. Yao, and G. Yang. 2015. "Recent Advances in Graphene/Polyamide 6 Composites: A Review." *RSC Adv*. 5:61688–61702.

Gissinger, J. R., B. D. Jensen, and K. E. Wise. 2017. "Modeling Chemical Reactions in Classical Molecular Dynamics Simulations." *Polymer* 92:211–217.

Gu, H., Y. Guo, S. Y. Wong, C. He, X. Li, and V. P. Shim. 2013. "Effect of Interphase and Strain-Rate on the Tensile Properties of Polyamide 6 Reinforced with Functionalized Silica Nanoparticles." *Compos. Sci. Technol.* 75:62–69.

Gustafson, P. A., F. A. Yapor Genao, B. A. Bednarcyk, and E. J. Pineda. 2019. *Integration of MAC/GMC into CalculiX, an Open Source Finite Element Code*. AIAA Scitech 2019 Forum. Reston, VA.

Hadden, C. M., B. D. Jensen, A. Bandyopadhyay, G. M. Odegard, B. Koo, and R. Liang. 2013. "Molecular Modeling of EPON-862/Graphite Composites: Interfacial Characteristics for Multiple Crosslink Densities." *Composites Science and Technology* 76:92–99.

Hadden, C., D. Klimek-McDonald, E. Pineda, J. King, A. Reichanadter, I. Miskioglu, S. Gowtham, and G. Odegard. 2015. "Mechanical Properties of Graphene Nanoplatelet/Carbon Fiber/Epoxy Hybrid Composites: Multiscale Modeling and Experiments." *Carbon N. Y.* 35:100–112.

Heinz, H. *IFF-R: Simulate Bond Breaking and Stress-Strain Curves up to Failure*. 2021. https://bionanostructures.com/interface-md/.

Heinz, H., T.-J. Lin, R. Kishore Mishra, and F. S. Emami. 2013. "Thermodynamically Consistent Force Fields for the Assembly of Inorganic, Organic, and Biological Nanostructures: The INTERFACE Force Field." *Langmuir* 23:1754–1765.

Höwer, D., S. Yu, T. M. Ricks, B. A. Bednarcyk, E. J. Pineda, B. Stier, S. Reese, and J.-W. Simon. 2019. "Weave Geometry Generation Avoiding Interferences for Mesoscale RVEs." *Journal of Materials Science & Technology* 5:2869–2882.

Huang, J., W. Ulrich, S. Schmauder, and S. Geier. 2011. "Micro-mechanical Modelling of Young's Modulus of Semi-crystalline Polyamide 6 (PA 6) and Elastomer Particle-modified-PA6." *Comput. Mater. Sci.* 50:1315–1319.

Hudson, S. D., D. D. Davis, and A. J. Lovinger. 1992. "Semicrystalline Morphology of Poly(aryl ether ether ketone)/poly(ether imide) Blends." *Macromolecules* 25:1759–1765.

Ivanov, D. A., B. Nysten, and A. M. Jonas. 1999. "Atomic Force Microscopy Imaging of Single Polymer Spherulites during Crystallization: Application to a Semi-Crystalline Blend." *Polymer* 40:5899–5905.

Jiang, Z., Y. Tang, J. Rieger, H. F. Enderle, D. Lilge, S. V. Roth, R. Gehrke, Z. Wu, Z. Li, and Y. Men. 2009. "Structural Evolution of Tensile Deformed High-Density Polyethylene at Elevated Temperatures: Scanning Synchrotron Small- and Wide-angle X-ray Scattering Studies." *Polymer* 50:4101–4111.

King, J. A., D. R. Klimek, I. Miskioglu, and G. M. Odegard. "Mechanical Properties of Graphene Nanoplatelet/Epoxy Composites." *J. Appl. Polym. Sci.* 92:4217–4223.

Liu, H., L. Hou, W. Peng, Q. Zhang, and X. Zhang. 2012. "Fabrication and Characterization of Polyamide 6-Functionalized Graphene Nanocomposite Fiber." *J. Mater. Sci.* 47: 8052–8060.

Liu, H., I. Y. Phang, L. Shen, S. Y. Chow, and W.-D. Zhang. 2004. "Morphology and Mechanical Properties of Multiwalled Carbon Nanotubes Reinforced Nylon-6 Composites." *Macro-molecules* 7:7214–7222.

Mayoral, B., E. Harkin-Jones, P. N. Khanam, M. A. AlMaadeed, M. Ouederni, A. R. Hamilton, and D. Sun. 2015. "Melt Processing and Characterisation of Polyamide 6/Graphene Nanoplatelet Composites." *RSC Adv.* 5:52395–52409.

Méndez, R., B. Constant, C. Garzon, M. Nisar, S. M. B. Nachtigall, and R. Quijada. 2017. "Barrier, Mechanical and Conductive Properties of Polycaprolactam Nanocomposites Containing Carbon-based Particles: Effect of the Kind of Particle." *Polymer* 130:10–16.

Mills, N., M. Jenkins, and S. Kukureka. 2020. *Plastics*. Amsterda, Netherlands: Elsevier.

Muggeo, V. M. R. 2003. "Estimating Regression Models with Unknown Break-points." *Stat. Med.* 22:3055–3071.

Murthy, N. S. 1991. "Metastable Crystalline Phases in Nylon 6." *Polym. Commun.* 32(10): 301–305.

Odegard, G. M., B. D. Jensen, S. Gowtham, J. Wu, J. He, and Z. Zhang. 2014. "Predicting Mechanical Response of Crosslinked Epoxy Using ReaxFF." *Chem. Phys. Lett.* 591:175–178.

Odegard, G. M., S. U. Patil, P. Deshpande, K. Kanhaiya, J. Winetrout, H. Heinz, S. Shah, and M. Maiaru. 2021. *Molecular Dynamics Modeling of Epoxy Resins using the Reactive Interface Force Field*.

Park, M., J.-u. Jang, J. H. Park, J., and S. Y. Kim. 2020. "Enhanced Tensile Properties of Multi-Walled Carbon Nanotubes Filled Polyamide 6 Composites Based on Interface Modification and Reactive Extrusion." *Polymers (Basel)* 92:997.

Patil, S. U., M. S. Radue, W. A. Pisani, P. Deshpande, H. Xu, H. Al Mahmud, T. Dumitrica, and G. M. Odegard. 2020. "Interfacial Characteristics between Flattened CNT Stacks and Polyimides: A Molecular Dynamics Study." *Computational Materials Science* 185:109970.

Phang, I. Y., J. Ma, L. Shen, T. Liu, and W.-D. Zhang. 2006. "Crystallization and Melting Behavior of Multi-walled Carbon Nanotube-reinforced Nylon-6 Composites." *Polym. Int*. 55:71–79.

Pineda, E. J., T. M. Ricks, B. A. Bednarcyk, and S. M. Arnold. 2021. *Benchmarking and Performance of the NASA Multiscale Analysis Tool. AIAA Scitech 2021 Forum*. Reston, VA.

Pisani, W. A., M. S. Radue, S. Chinkanjanarot, B. A. Bednarcyk, E. J. Pineda, K. Waters, R. Pandey, J. A. King, and G. M. Odegard. 2019. "Multiscale Modeling of PEEK Using Reactive Molecular Dynamics Modeling and Micromechanics." *Polymer* 163:96–105.

Pisani, W. A., M. S. Radue, S. U. Patil, and G. M. Odegard. 2021. "Interfacial Modeling of Flattened CNT Composites with Cyanate Ester and PEEK Polymers." *Composites Part B: Engineering* 211:108672.

Pisani, W. A., D. N. Wedgeworth, M. R. Roth, J. K. Newman, and M. K. Shukla. 2021. "Computational Prediction of Mechanical Properties of PA6-Graphene/Carbon Nanotube Nanocomposites." *The Journal of Physical Chemistry C* 125:15569–15578.

Plimpton, S. 1995. "Fast Parallel Algorithms for Short-Range Molecular Dynamics." *J. Comput. Phys.* 117:1–19.

Qian, D., E. C. Dickey, R. Andrews, and T. Rantell. 2000. "Load Transfer and Deformation Mechanisms in Carbon Nanotube-Polystyrene Composites." *Appl. Phys. Lett*. 76:2868–2870.

Radue, M. S., B. D. Jensen; S. Gowtham, D. R. Klimek-McDonald, J. A. King, and G. M. Odegard. 2018. "Comparing the Mechanical Response of Di-, Tri-, and Tetra-Functional Resin Epoxies with Reactive Molecular Dynamics." *J. Polym. Sci. Part B Polym. Phys*. 56:255–264.

Radue, M. S., V. Varshney, J. W. Baur, A. K. Roy, and G. M. Odegard. 2018. "Molecular Modeling of Cross-Linked Polymers with Complex Cure Pathways: A Case Study of Bismaleimide Resins." *Macromolecules* 51:1830–1840.

Ricks, T. M., B. Farrokh, B. A. Bednarcyk, and E. J. Pineda. 2019. *A Comparison of Different Modeling Strategies for Predicting Effective Properties of 3D Woven Composites*. AIAA Scitech 2019 Forum. Reston, VA.

Shan, G. F., W. Yang, M. bo Yang, B. hu Xie, J. min Feng, and Q. Fu. 2007. "Effect of Temperature and Strain Rate on the Tensile Deformation of Polyamide 6." *Polymer* 48:2958–2968.

Shan, G. F., W. Yang, M. bo Yang, B. hu Xie, Q. Fu, and Y. W. Mai. 2009. "Investigation on Tensile Deformation Behavior of Semi-crystalline Polymers." *J. Macromol. Sci. Part B Phys.* 48:799–811.

Shao, W., Q. Wang, F. Wang, and Y. Chen. 2006. "The Cutting of Multi-Walled Carbon Nanotubes and their Strong Interfacial Interaction with Polyamide 6 in the Solid State." *Carbon N. Y.* 44:2708–2714.

Shibukawa, T., V. Gupta, R. Turner, J. Dillon, and A. Tobolsky.962. "Temperature Dependence of Shear Modulus and Density of Nylon-6." *Text. Res. J.* 32:1011–1012.

Strobl, G. 2006. "Crystallization and Melting of Bulk Polymers: New Observations, Conclusions and a Thermodynamic Scheme." *Prog. Polym. Sci.* 31:398–442.

Stukowski, A. 2010. "Visualization and Analysis of Atomistic Simulation Data with OVITO-the Open Visualization Tool." *Model. Simul. Mater. Sci. Eng.* 18:5012.

Su, C. H., W. R. Wu, C. Y. Chen, C. J. Su, W. T. Chuang, K. F. Liao, S. H. Chen, A. C. Su, and U. S. Jeng. 2016. "Nanograin Nucleation at the Growth Front in Melt Crystallization of Syndiotactic Polystyrene." *Polymer* 105:414–421.

Sun, L., J. T. Yang, G. Y. Lin, and M. Q. Zhong. 2007. "Crystallization and Thermal Properties of Polyamide 6 Composites Filled with Different Nanofillers." *Mater. Lett.* 61:3963–3966.

Tahreen, N., and A. Masud. 2013. "A Molecular Dynamics Simulation Study of the Mechanical Properties of Carbon-Nanotube Reinforced Nylon 6 Composite." *Int. J. Manuf. Mater. Mech. Eng.*3:62–73.

Tashiro, K., and H. Tadokoro. 1981. "Calculation of Three-Dimensional Elastic Constants of Polymer Crystals. 3. α and γ Forms of Nylon 6." *Macromolecules* 14:781–785.

Tomasi, J., W. A. Pisani, S. Chinkanjanarot, A. S. Krieg, D. Jaszczak, E. J. Pineda, B. A. Bednarcyk, S. Miller, J. A. King, I. Miskioglu et al. 2019. *Modeling-Driven Damage Tolerant Design of Graphene Nanoplatelet/Carbon Fiber/Epoxy Hybrid Composite Panels for Full-Scale Aerospace Structures*. AIAA Scitech 2019 Forum. Reston, VA.

Wang, R., H.-C. Kuan, A. Qiu, X. Su, and J. Ma. 2020. "A Facile Approach to the Scalable Preparation of Thermoplastic/Carbon Nanotube Composites." *Nanotechnology* 31:195706.

Wang, Y., J. D. Beard, K. E. Evans, and O. Ghita. 2016. "Unusual Crystalline Morphology of Poly Aryl Ether Ketones (PAEKs)." *RSC Adv.* 6:3198–3209.

Winetrout, J. J., K. Kanhaiya, G. Sachdeva, R. Pandey, B. Damirchi, A. van Duin, G. Odegard, and H. Heinz. 2021. *Implementing Reactivity in Molecular Dynamics Simulations with the Interface Force Field (IFF-R) and Other Harmonic Force Fields*. https://doi.org/10.48550/arXiv.2107.14418.

Xu, C., Z. Jia, D. Wu, Q. Han, and T. Meek. 2006. "Fabrication of Nylon-6/Carbon Nanotube Composites." *J. Electron. Mater.* 35:954–957.

Yu, X., X. Dong, Z. Song, and J. Gui. 2020. "Fabrication of Polyamide 6 Nanocomposites Reinforced by the Exfoliated Graphene." *Plast. Rubber Compos.* 49:281–288.

Zhou, L., H. Liu, and X. Zhang. 2015. "Graphene and Carbon Nanotubes for the Synergistic Reinforcement of Polyamide 6 Fibers. *J. Mater. Sci.* 50:2797–2805.

Zhu, Q., V. Sharma, A. R. Oganov, and R. Ramprasad. 2014. "Predicting Polymeric Crystal Structures by Evolutionary Algorithms." *J. Chem. Phys.* 141:154102.

Abbreviations

CNT	Carbon nanotubes
CNT/G	Carbon nanotubes/graphene
CPK	Corey-Pauling-Koltun
G	Graphene
GNP	Graphene nanoplatelet
IFF	INTERFACE force field
IFF-R	Reactive INTERFACE force field
MAC/GMC	Micromechanics Analysis Code/Generalized Method of Cells
MD	Molecular dynamics
MSGMC	MultiScale Generalized Method of Cells
NASA	National Aeronautics and Space Administration
NPT	Molecular dynamics ensemble, N is constant number of particles, P is constant pressure, T is constant temperature
NVT	Molecular dynamics ensemble, N is constant number of particles, V is constant volume, T is constant temperature
PA6	Polyamide 6
PEEK	Polyetheretherketone
RUC	Repeating unit cell

REPORT DOCUMENTATION PAGE

Form Approved
OMB No. 0704-0188

1. REPORT DATE	2. REPORT TYPE	3. DATES COVERED *(From - To)*
March 2023	Final Report	FY21—FY22

4. TITLE AND SUBTITLE

Exploration of Two Polymer Nanocomposite Structure-Property Relationships Facilitated by Molecular Dynamics Simulation and Multiscale Modeling

5a. CONTRACT NUMBER

5b. GRANT NUMBER

5c. PROGRAM ELEMENT NUMBER

PE 0602144A

6. AUTHOR(S)

William A. Pisani, Dane N. Wedgeworth, Michael R. Roth, John K. Newman, and Manoj K. Shukla

5d. PROJECT NUMBER

Project Number 497006

5e. TASK NUMBER

Task Number 5L9C47

5f. WORK UNIT NUMBER

7. PERFORMING ORGANIZATION NAME(S) AND ADDRESS(ES)

(see reverse)

8. PERFORMING ORGANIZATION REPORT NUMBER

ERDC TR-23-4

9. SPONSORING/MONITORING AGENCY NAME(S) AND ADDRESS(ES)

Geotechnical and Structures Laboratory
US Army Engineer Research and Development Center
Research Group, CEERD-GMR
3909 Halls Ferry Road
Vicksburg, MS 39180-6199

10. SPONSOR/MONITOR'S ACRONYM(S)

GSL

11. SPONSOR/MONITOR'S REPORT NUMBER(S)

12. DISTRIBUTION/AVAILABILITY STATEMENT

DISTRIBUTION STATEMENT A. Approved for public release; distribution is unlimited.

13. SUPPLEMENTARY NOTES

14. ABSTRACT

Polyamide 6 (PA6) is a semi-crystalline thermoplastic used in many engineering applications due to good strength, stiffness, mechanical damping, wear/abrasion resistance, and excellent performance-to-cost ratio. In this report, two structure-property relationships were explored. First, carbon nanotubes (CNT) and graphene (G) were used as reinforcement molecules in simulated and experimentally prepared PA6 matrices to improve the overall mechanical properties. Molecular dynamics (MD) simulations with INTERFACE and reactive INTERFACE force fields (IFF and IFF-R) were used to predict bulk and Young's moduli of amorphous PA6-CNT/G nanocomposites as a function of CNT/G loading. The predicted values of Young's modulus agree moderately well with the experimental values. Second, the effect of crystallinity and crystal form (α/γ) on mechanical properties of semi-crystalline PA6 was investigated via a multiscale simulation approach. The National Aeronautics and Space Administration, Glenn Research Center's micromechanics software was used to facilitate the multiscale modeling. The inputs to the multiscale model were the elastic moduli of amorphous PA6 as predicted via MD and calculated stiffness matrices from the literature of the PA6 α and γ crystal forms. The predicted Young's and shear moduli compared well with experiment.

15. SUBJECT TERMS

Carbon, Graphene, Micromechanics, Molecular dynamics—Computer simulation, Multiscale modeling, Nanocomposites (Materials), Thermoplastics

16. SECURITY CLASSIFICATION OF:			17. LIMITATION OF ABSTRACT	18. NUMBER OF PAGES	19a. NAME OF RESPONSIBLE PERSON
a. REPORT	b. ABSTRACT	c. THIS PAGE			Manoj K. Shukla
Unclassified	Unclassified	Unclassified	SAR	40	19b. TELEPHONE NUMBER *(Include area code)* 601-634-5431

7. PERFORMING ORGANIZATION NAME(S) AND ADDRESS(ES) (continued)

Environmental Laboratory
US Army Engineer Research and Development Center
3909 Halls Ferry Road
Vicksburg, MS 39180-6199

Geotechnical and Structures Laboratory
US Army Engineer Research and Development Center
3909 Halls Ferry Road
Vicksburg, MS 39180-6199

Oak Ridge Institute for Science and Education
1299 Bethel Valley Road
Oak Ridge, TN 37830-8007